超新星理論開発

2017.5.22 @ 岡山大学
東京理科大学理工学部 鈴木英之
共同研究者：中里、持田、新納ほか

超新星背景ニュートリノ

過去の超新星で放出されたニュートリノが、宇宙膨張により赤方偏移しながら、宇宙空間を (ほぼ) 一様に満たしているはず。

- 超新星発生率
- 個々の超新星で放出されるニュートリノのエネルギースペクトル
- 宇宙膨張則

$\Rightarrow$ 現在の超新星背景ニュートリノエネルギースペクトル

超新星ニュートリノデータベース

http://asphwww.ph.noda.tus.ac.jp/snn/　Nakazato *et al.*, ApJS205 (2013) 2

数種類の親星モデル $(M = 13, 20, 30, 50M_\odot, Z = 0.02(Z_\odot), 0.004(0.2Z_\odot))$

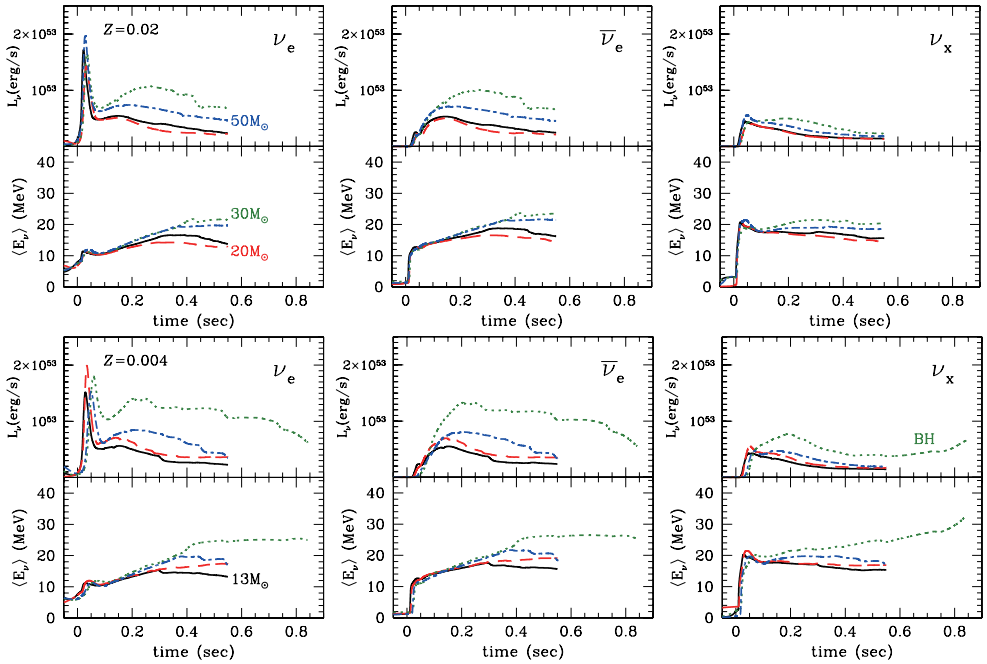

Figure 12. Luminosities (upper plots) and average energies (lower plots) of the emitted neutrinos as a function of time after the bounce from the νRHD simulations. The panels correspond, from left to right, to ν_e, $\bar{\nu}_e$, and ν_x ($= \nu_\mu$, ν_τ, $\bar{\nu}_\mu$, $\bar{\nu}_\tau$). The results for the models with metallicity $Z = 0.02$ are shown in the top panels, and those for the models with $Z = 0.004$ are shown in the bottom panels. In all panels, solid, dashed, dotted, and dot-dashed lines correspond to the models with initial mass $M_{\rm init} = 13\,M_\odot$, $20\,M_\odot$, $30\,M_\odot$, and $50\,M_\odot$, respectively. "BH" means a black-hole-forming model with $M_{\rm init} = 30\,M_\odot$ and $Z = 0.004$; its end point corresponds to the moment of black hole formation.

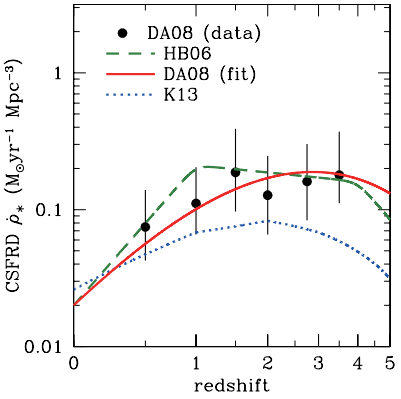

宇宙星形成率密度

$\dot{\rho}_*(z)$

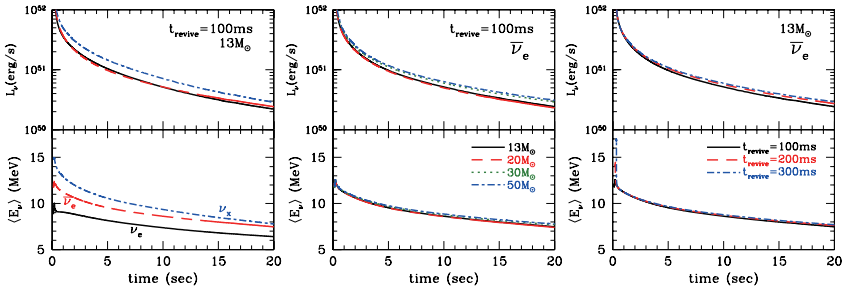

Figure 13. Same as Figure 12 but from the PNSC simulations. In the left panel, signals of ν_e (solid lines), $\bar{\nu}_e$ (dashed lines), and ν_x (dot-dashed lines) are shown for the model with ($M_{\rm init}$, Z, $t_{\rm revive}$) = (13 $M_\odot$, 0.02, 100 ms). In the central panel, $\bar{\nu}_e$ signals are shown for the models with (Z, $t_{\rm revive}$) = (0.02, 100 ms) and $M_{\rm init}$ = 13 $M_\odot$ (solid lines), 20 $M_\odot$ (dashed lines), 30 $M_\odot$ (dotted lines), and 50 $M_\odot$ (dot-dashed lines). In the right panel, $\bar{\nu}_e$ signals are shown for the models with ($M_{\rm init}$, Z) = (13 $M_\odot$, 0.02) and $t_{\rm revive}$ = 100 ms (solid lines), 200 ms (dashed lines), and 300 ms (dot-dashed lines).

Nakazato et al.(2013)　より

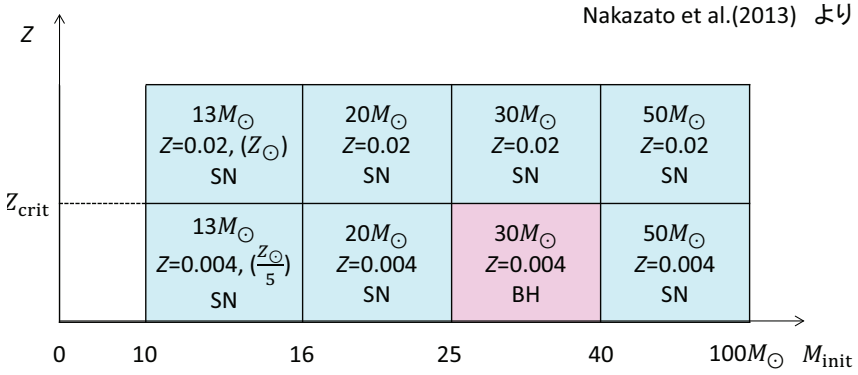

IMF 初期質量関数：Salpeter 型 $\psi_{\rm IMF}(M) \propto M^{-2.35}$

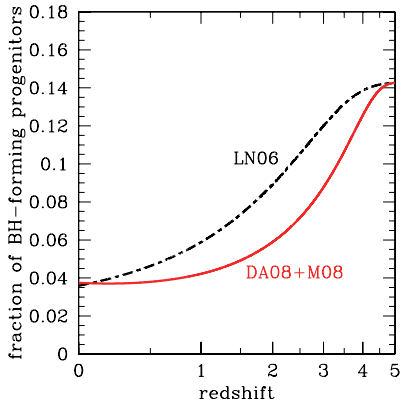

ブラックホール形成イベントの割合

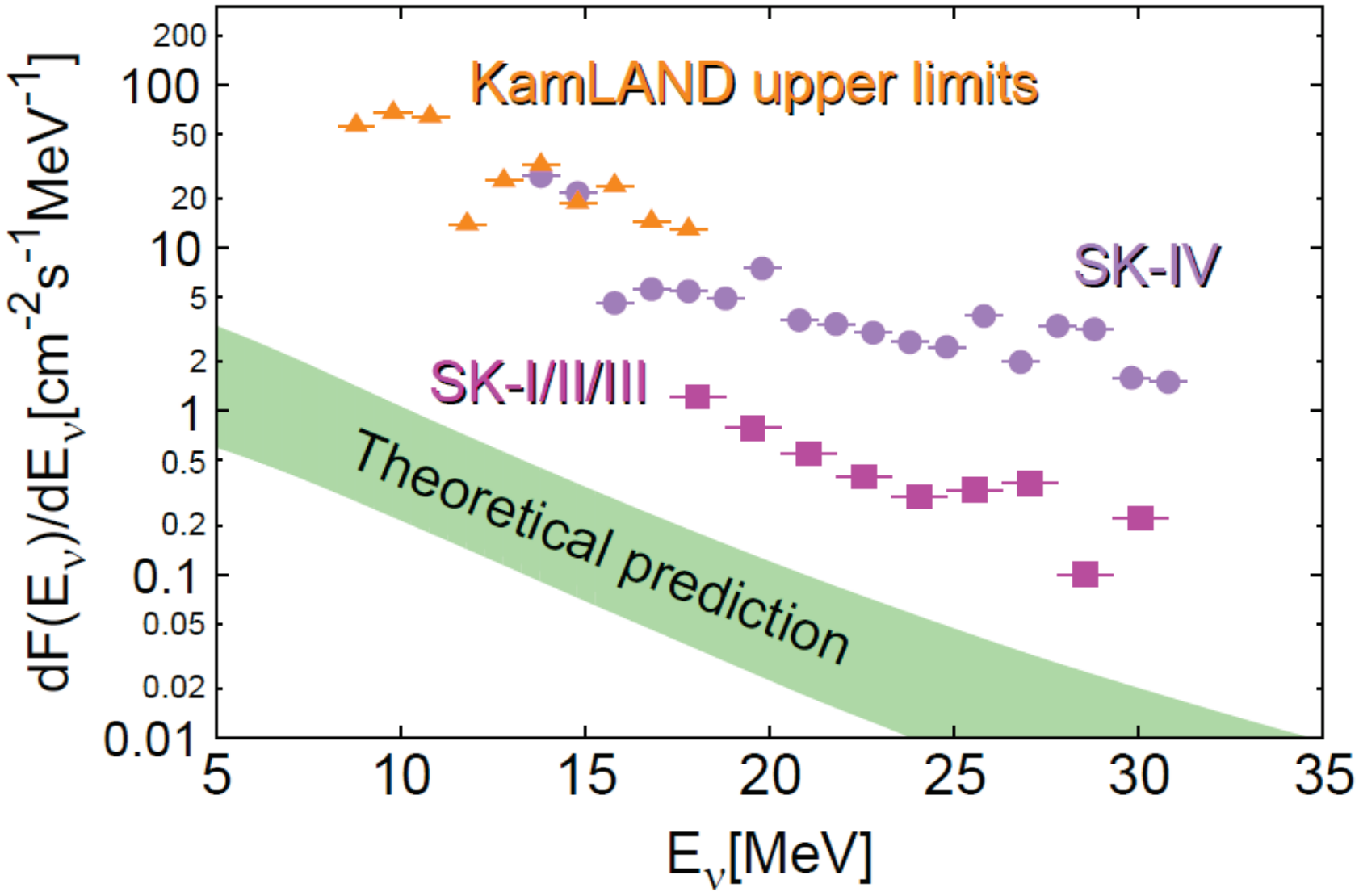

90% C.L. differential upper limits on $\bar{\nu}_e$ flux of SRNs. The squares, circles and triangles are results for Super-Kamiokande, Super-Kamiokande with a neutron-tagging and KamLAND. Dashed and dotted lines correspond to our theoretical models with maximum and minimum values of SRN event rate, respectively.

Nakazato *et al.*, 2015

Garching グループの超新星モデルを使った評価

A. Priya and C. Lunardini, 2017

金属量の進化は考慮してない。

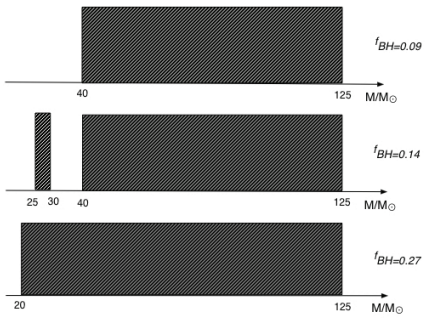

Figure 1: Different scenarios for the intervals of progenitor mass where direct black hole formation can be expected (shaded areas). The legend shows the corresponding fractions of BHFC, f_{BH}.

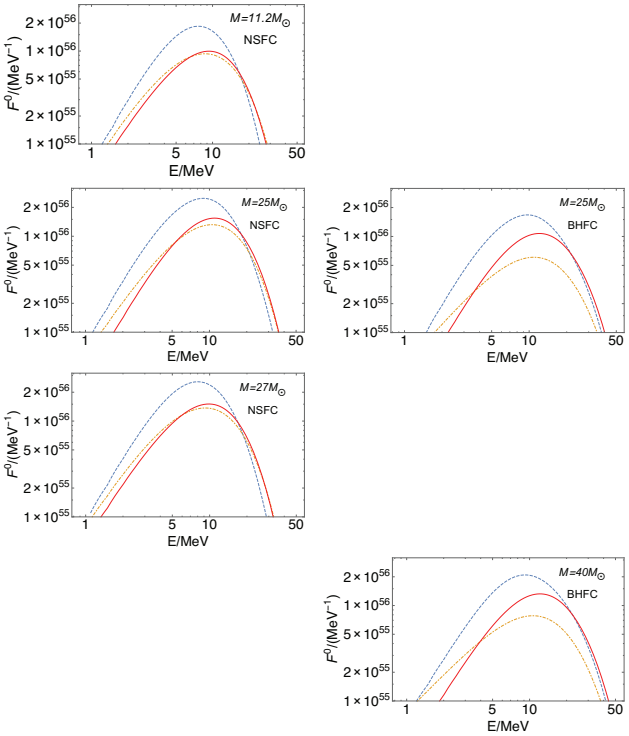

Figure 2: The time-integrated spectra at production (before oscillations), for different neutrino species and different progenitor masses, M. The panes are ordered vertically with increasing M (legends). Left column: successful explosion (NSFC); right column: Black-hole forming collapses (BHFC). The blue dashed, red solid and yellow dot-dashed lines correspond to the ν_e, $\bar{\nu}_e$ and ν_x spectra, respectively.

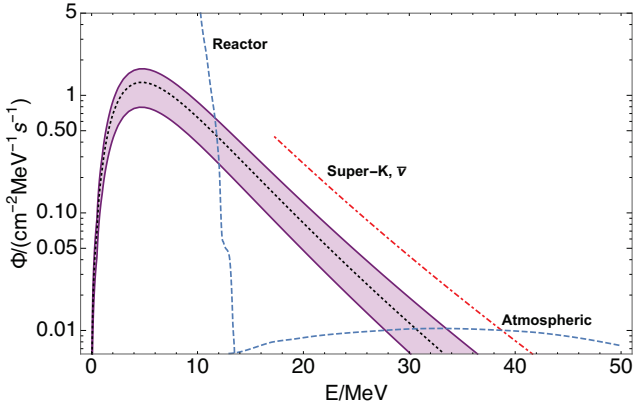

Figure 5: Summary: the Diffuse Supernova Neutrino Background (total of neutron-star-forming- and black-hole-forming- collapses), for $\bar{p} = 0.68$, with uncertainties due to astrophysical inputs and to the fraction of black hole-forming collapses (shaded area). Shown is the predicted flux for the Fiducial (dotted line), Low and High cases (solid lines), as in Table 2. Background $\bar{\nu}_e$ fluxes are shown as dashed lines: from nuclear reactors at lower energy (taken from [51]) and from the atmosphere at higher energy [52], for the Kamioka site. For comparison, we also show a signal flux (dot-dashed line, same spectrum as the Fiducial case) that would saturate the current Super-Kamiokande upper bound [6] (see text).

⇒ 中里モデルと同等のフラックス

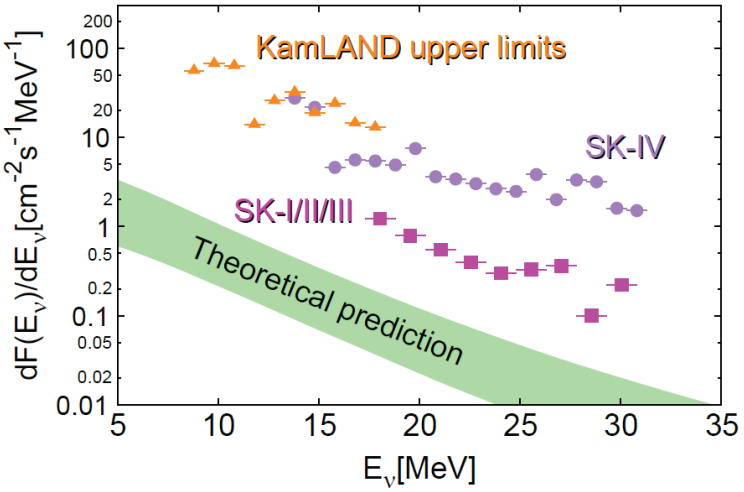

Nakazato *et al.*, 2015

星によって、放出される超新星ニュートリノの量、スペクトルは異なる。
(初期) 質量 M、金属量 Z によって、コアの密度分布などが異なる。

$$\Rightarrow \frac{dN_\nu(E'_\nu, M, Z)}{dE'_\nu}$$

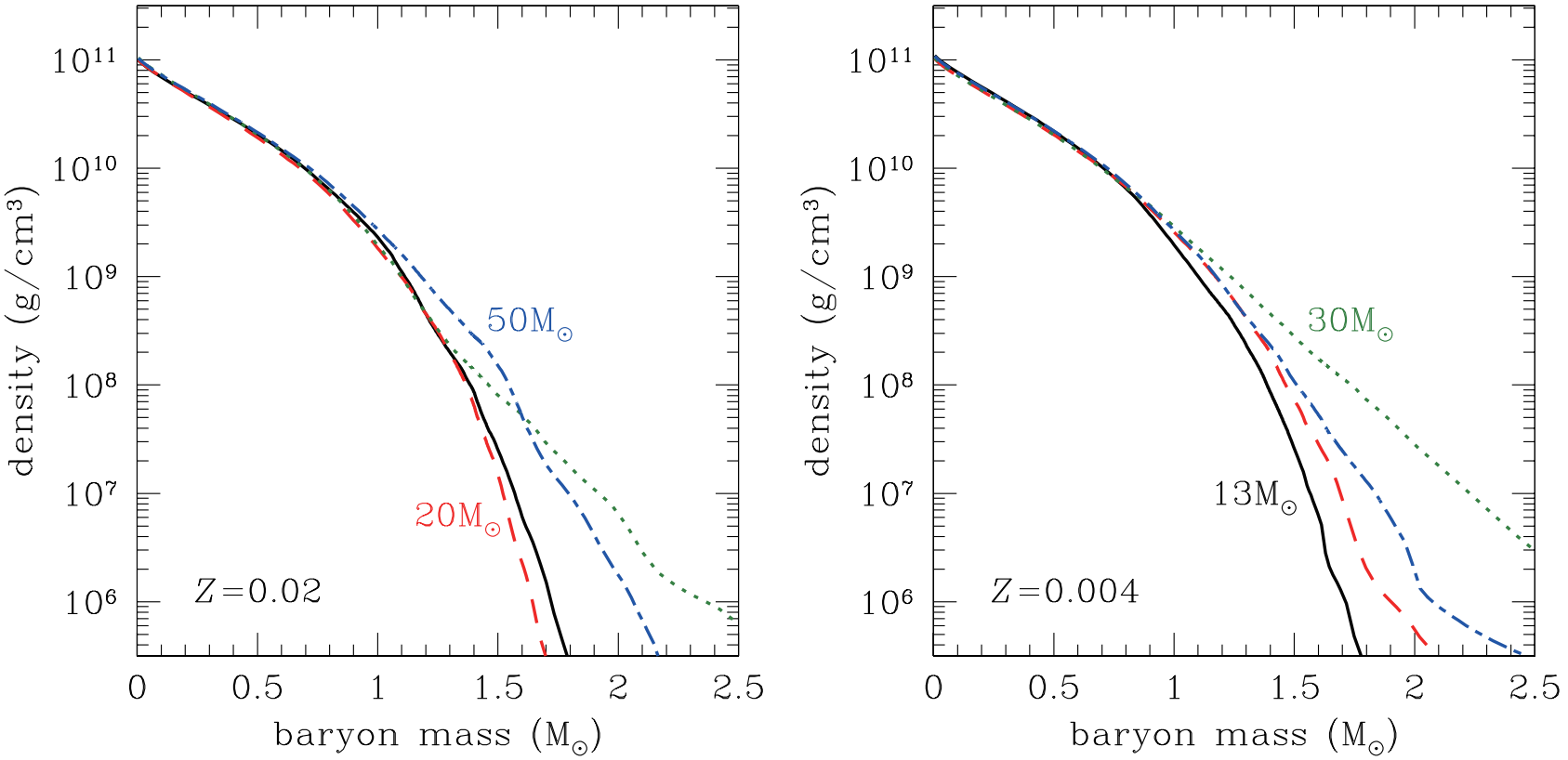

Figure 4. Density profiles at times with the central density of 10^{11} g cm^{-3} for progenitor models with metallicity $Z = 0.02$ (left panel) and 0.004 (right panel). In both panels, solid, dashed, dotted, and dot-dashed lines correspond to the models with initial mass $M_{\rm init} = 13\,M_\odot$, $20\,M_\odot$, $30\,M_\odot$, and $50\,M_\odot$, respectively.
(A color version of this figure is available in the online journal.)

M, Z が異なる星の密度分布：Nakazato *et al.*, 2013

Müller らによる親星の密度構造から重力崩壊後の振る舞いを評価する球対称モデル

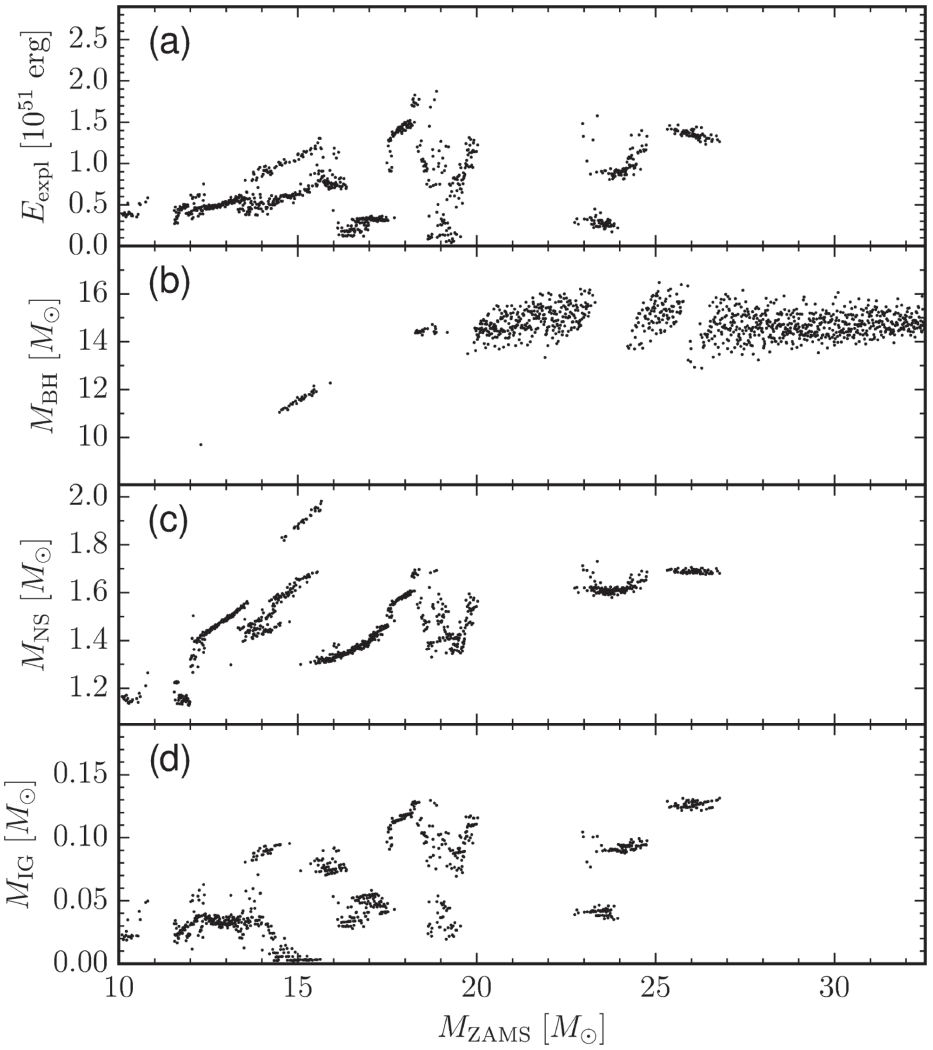

Figure 2. Explosion energy ($E_{\rm expl}$, panel a), gravitational remnant masses for black holes ($M_{\rm BH}$, panel b), neutron stars ($M_{\rm NS}$, panel c), and the iron-group mass ($M_{\rm IG}$, panel d) as a function of ZAMS mass for the standard case. Note that there is a gap in our set of progenitors around 11 $M_\odot$; missing data points in this region are not indicative of black hole formation.

$$\xi_M \equiv \frac{M/M_\odot}{r(M)/1000\mathrm{km}}$$

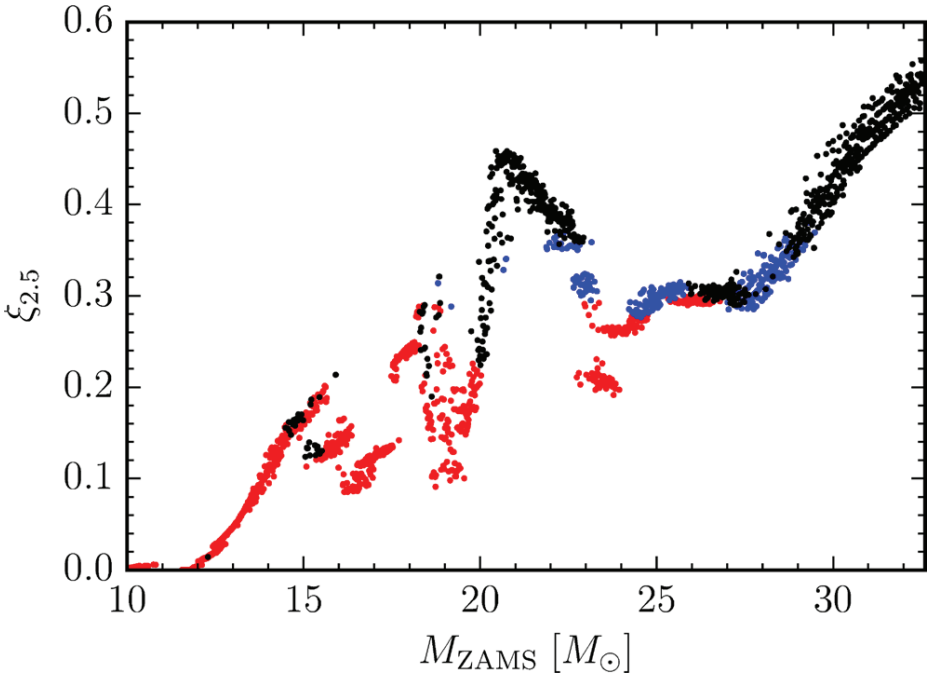

Figure 6. Compactness parameters $\xi_{2.5}$ for exploding (red) and non-exploding (black) models as a function of ZAMS mass. Blue dots denote models where shock revival is initiated, but the explosion eventually fails because the diagnostic energy becomes negative as the shock propagates out or the neutron star mass exceeds the maximum neutron star mass due to ongoing accretion in the explosion phase.

B. Müller *et al.*, 2016

現実的な核力モデルを用いた新しい状態方程式数値テーブル

富樫、中里、鷹野、鈴木、山室、竹原, 2017

- 一様核物質：クラスター変分法（2 体クラスター近似）：2 体力 AV18 ＋ 3 体力 UIX, 3 体力の不定性を利用し、原子核経験値を再現
- 非一様核物質：Thomas-Fermi（TF）近似: Wigner-Seitz 格子内の自由エネルギーを最小化 (Shen EOS の手法を踏襲)

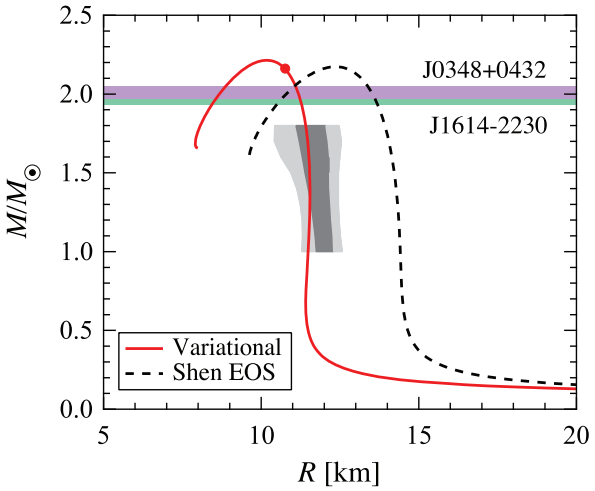

EOS	Togashi	Shen	LS220
K[MeV]	245	281	220
$E_{\rm sym}$[MeV]	30.0	36.9	28.6
L[MeV]	30	111	73.8
n_0[fm^{-3}]	0.16	0.145	0.155
E_0[MeV]	16.1	16.3	16.0
$M_{\rm NSmax}[M_\odot]$	2.21	2.23	2.06

Fig. 1. (Color online.) Mass–radius relation of neutron stars calculated with the present EOS. The filled circle represents the neutron star for which the central density is equal to the critical density $n_{\rm c}$. The horizontal green and purple bands show the masses of PSRs J1614-2230 [25] and J0348+0432 [26]. The shaded region indicates the mass–radius region suggested in Ref. [16]. The mass–radius relation with the Shen EOS is also shown.

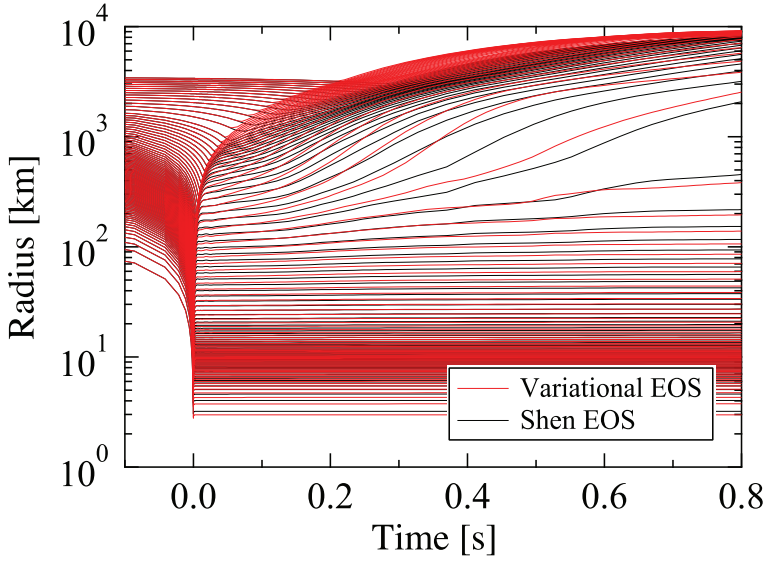

Fig. 5 The trajectories of the mass mesh in the radius of the core of a $15M_\odot$ star as functions of time with our SN-EOS. Also shown are those with the Shen EOS.

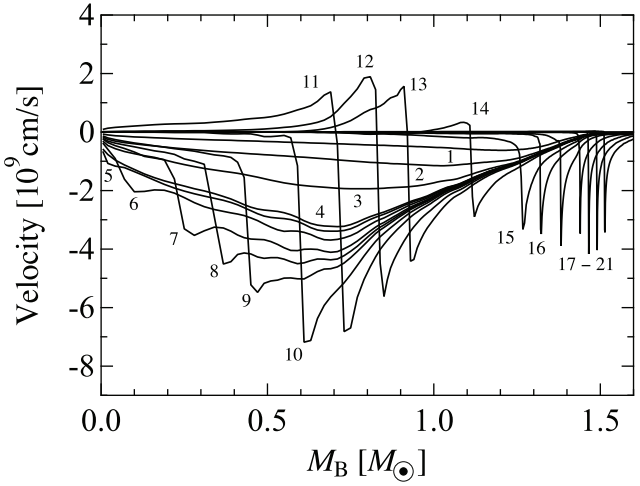

Fig. 11 The velocity profiles at selected times as functions of the baryon mass coordinate $M_{\rm B}$. The numbers denote the times explained in the text.

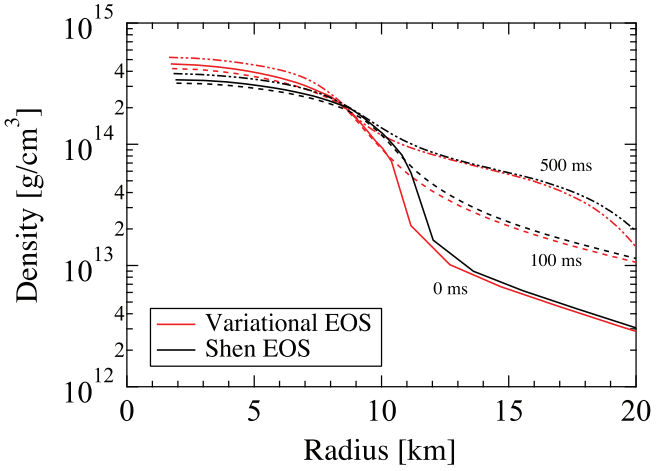

Fig. 12 The density profiles at $t_{\rm pb} = 0, 100$ and 500 ms as functions of the radius. The results with the Shen EOS are also shown.

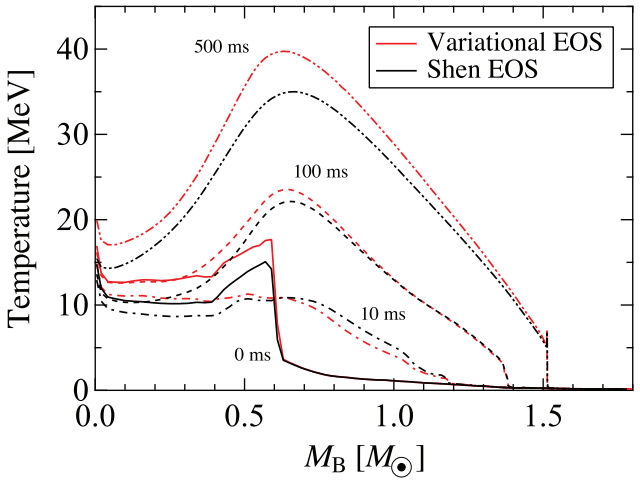

Fig. 16 The temperature profiles at $t_{\rm pb} = 0, 10, 100$ and 500 ms as functions of the baryon mass coordinate $M_{\rm B}$. The results with the Shen EOS are also shown.

原始中性子星の冷却計算

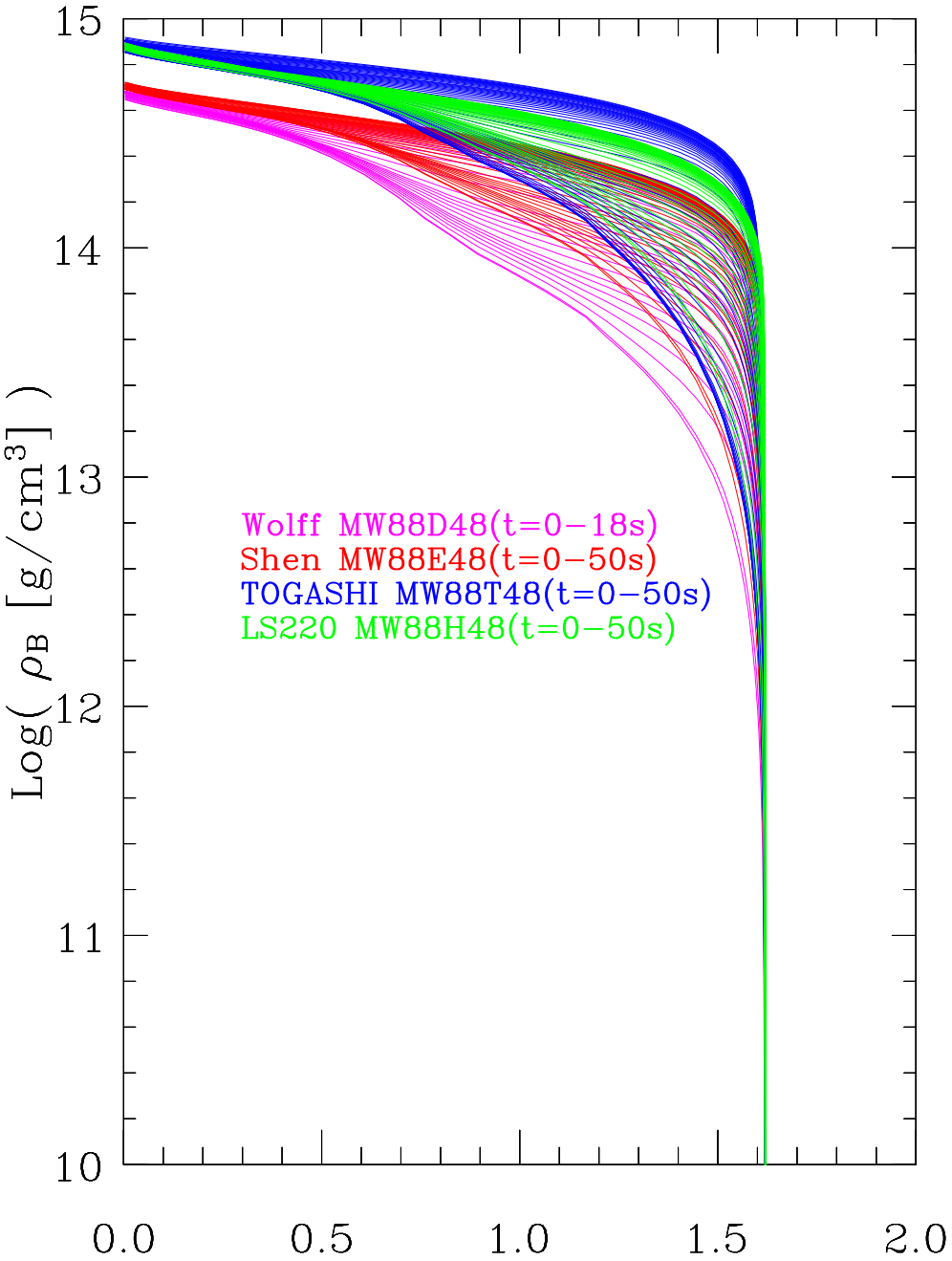

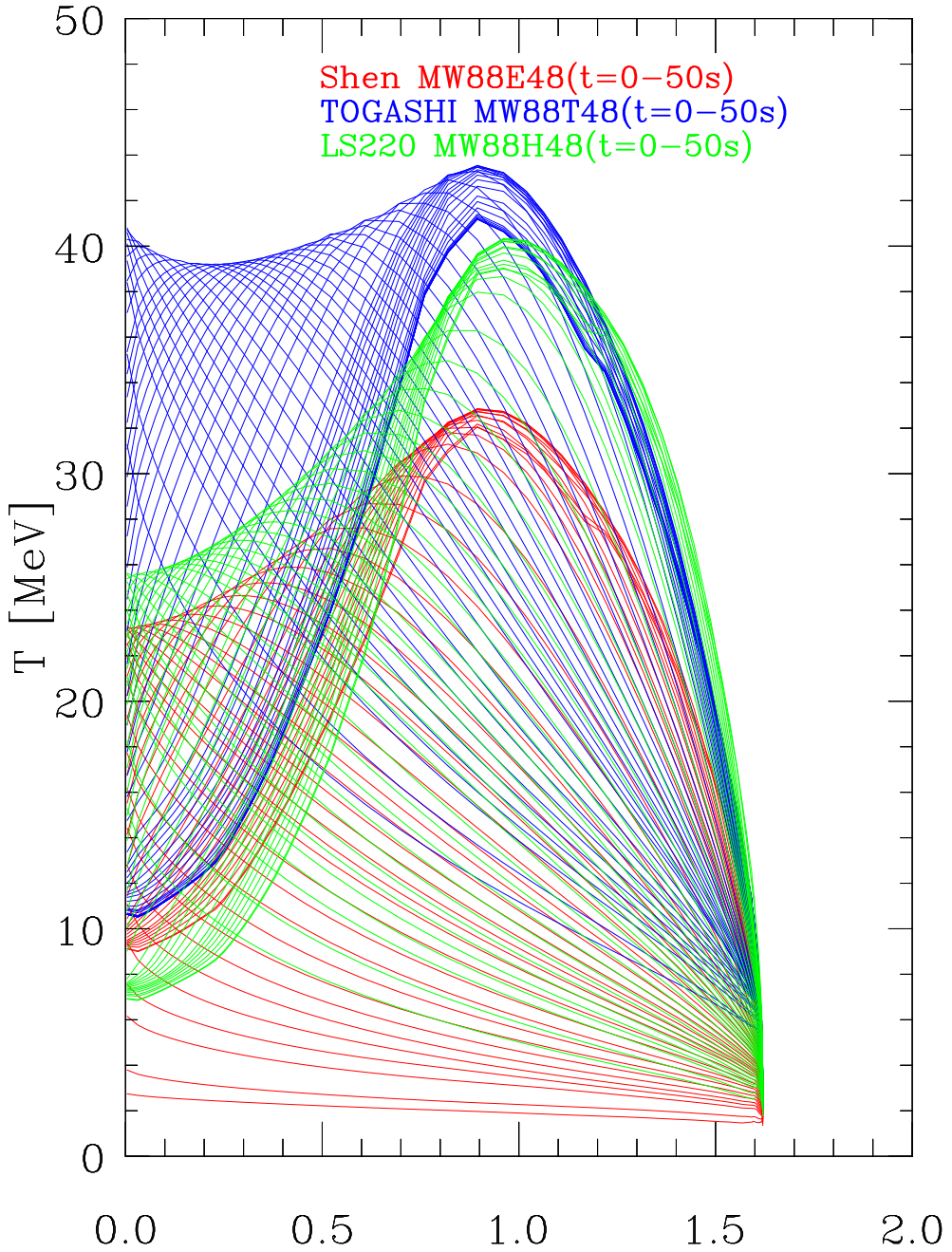

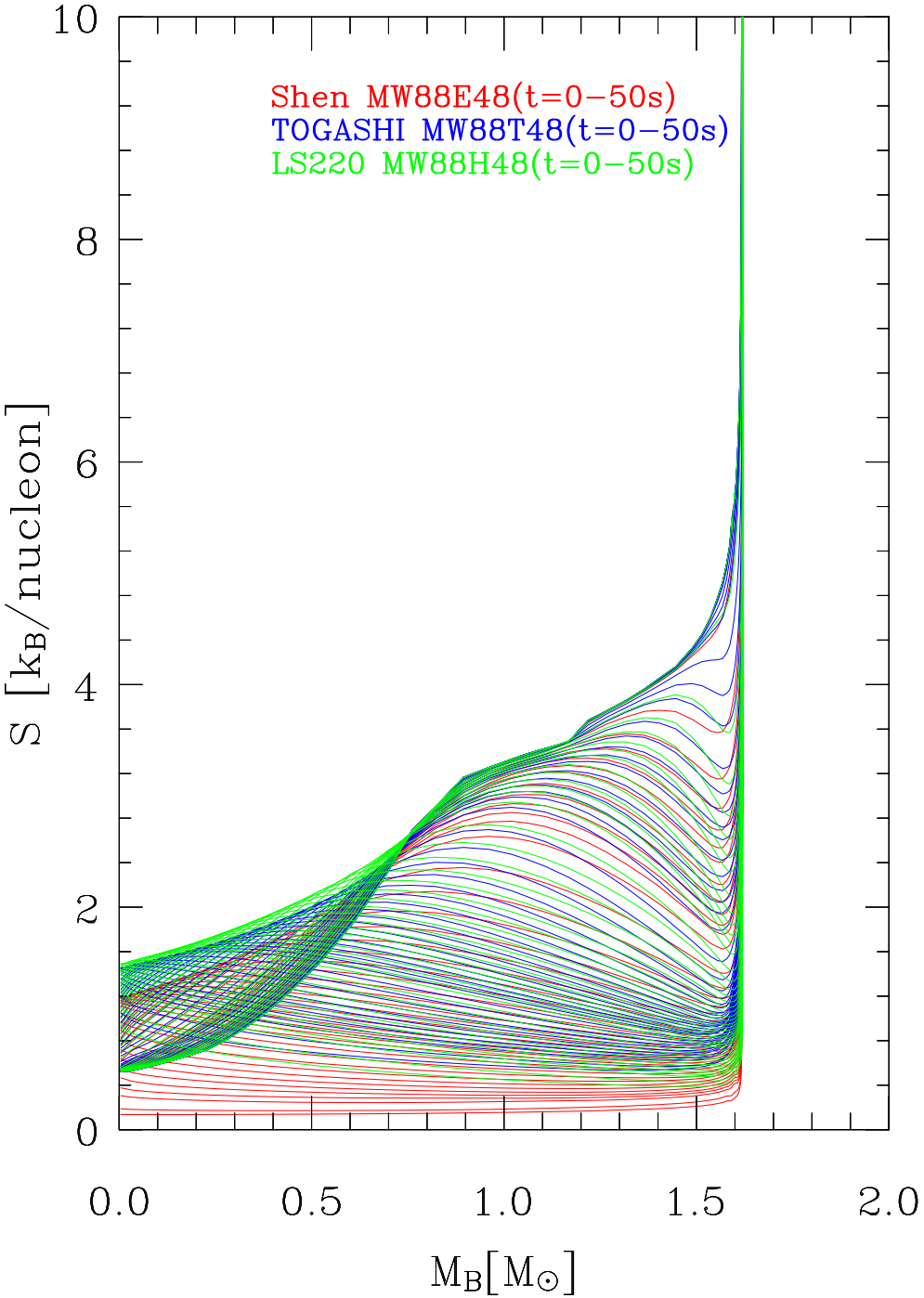
Shen MW88E48(t=0−50s)
TOGASHI MW88T48(t=0−50s)
LS220 MW88H48(t=0−50s)
S [k_B/nucleon]
M_B[M_⊙]
0
2
4
6
8
10
0.0
0.5
1.0
1.5
2.0

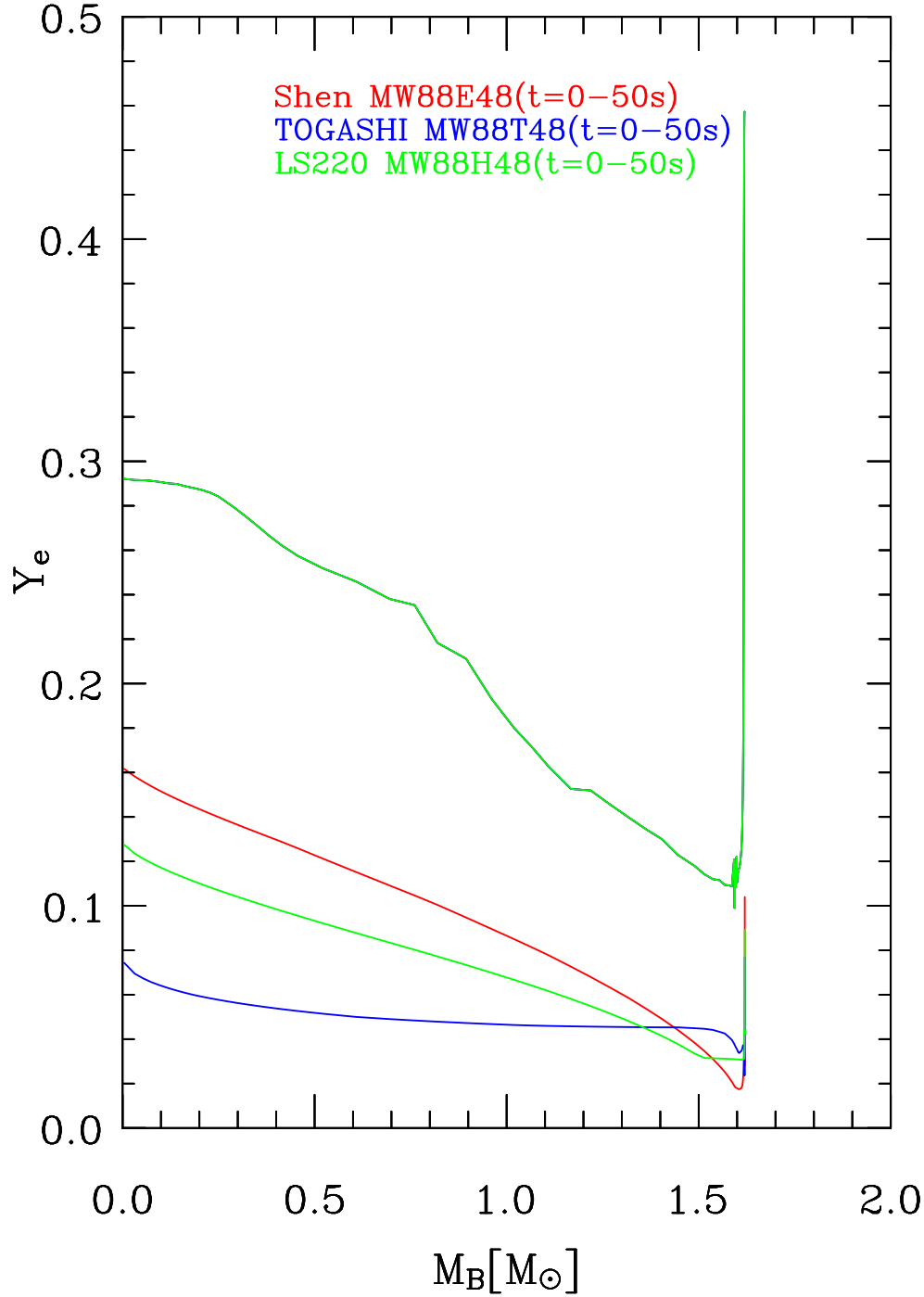
Shen MW88E48(t=0−50s)
TOGASHI MW88T48(t=0−50s)
LS220 MW88H48(t=0−50s)
Y_e
M_B[M_⊙]
0.0
0.1
0.2
0.3
0.4
0.5
0.0
0.5
1.0
1.5
2.0

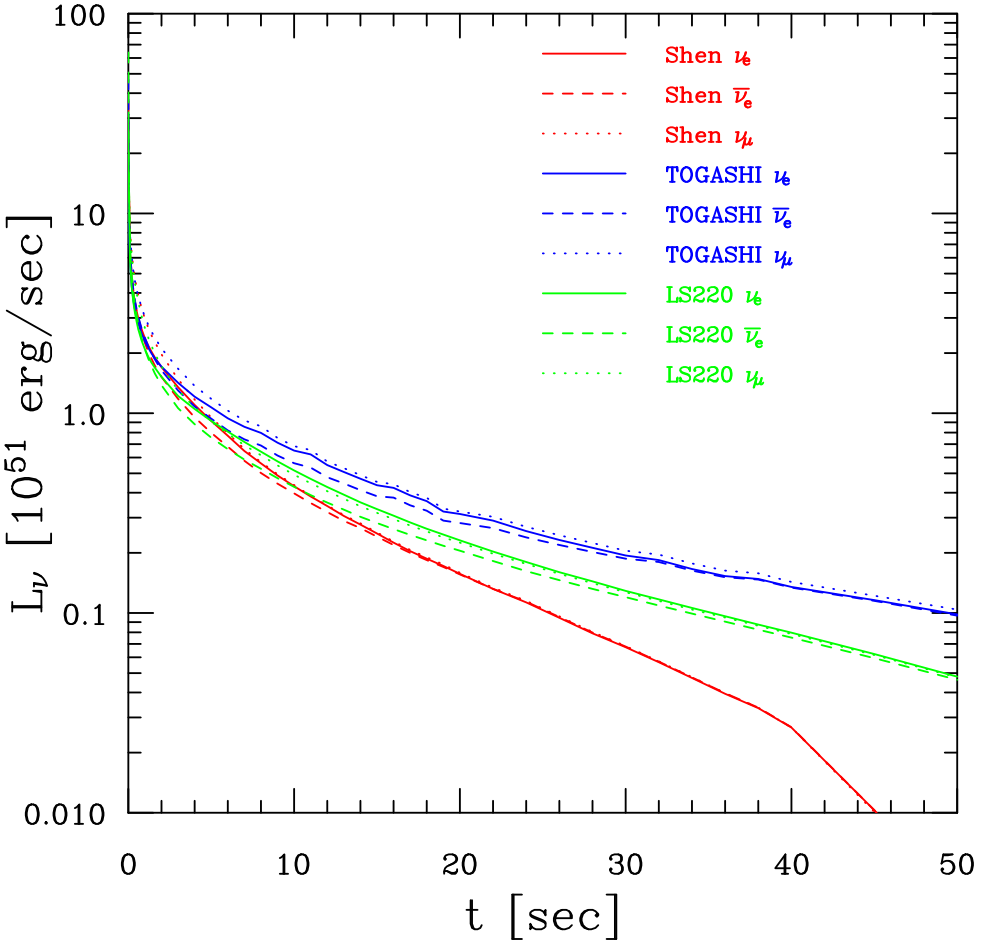
100
10
1.0
0.1
0.010
0
10
20
30
40
50
L_ν [10^{51} erg/sec]
t [sec]
Shen ν_e
Shen $\bar{\nu}_e$
Shen ν_μ
TOGASHI ν_e
TOGASHI $\bar{\nu}_e$
TOGASHI ν_μ
LS220 ν_e
LS220 $\bar{\nu}_e$
LS220 ν_μ

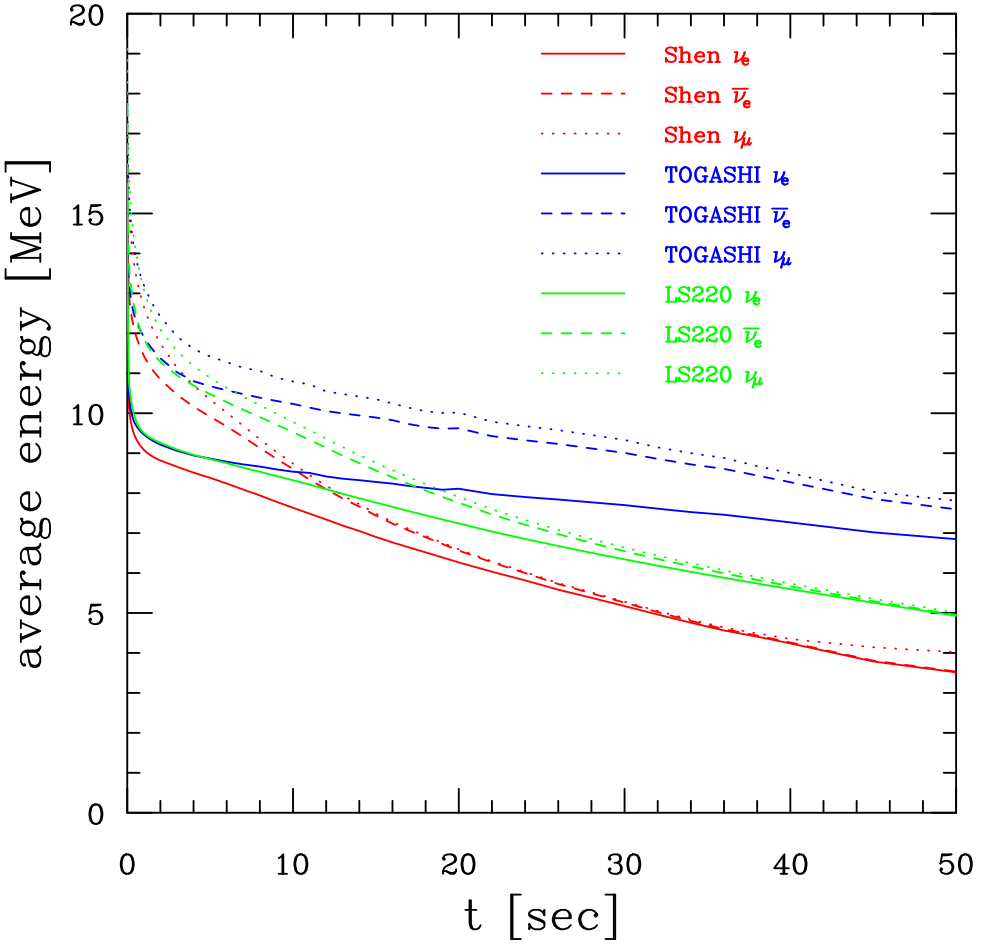
20
15
10
5
0
0
10
20
30
40
50
average energy [MeV]
t [sec]
Shen ν_e
Shen $\bar{\nu}_e$
Shen ν_μ
TOGASHI ν_e
TOGASHI $\bar{\nu}_e$
TOGASHI ν_μ
LS220 ν_e
LS220 $\bar{\nu}_e$
LS220 ν_μ

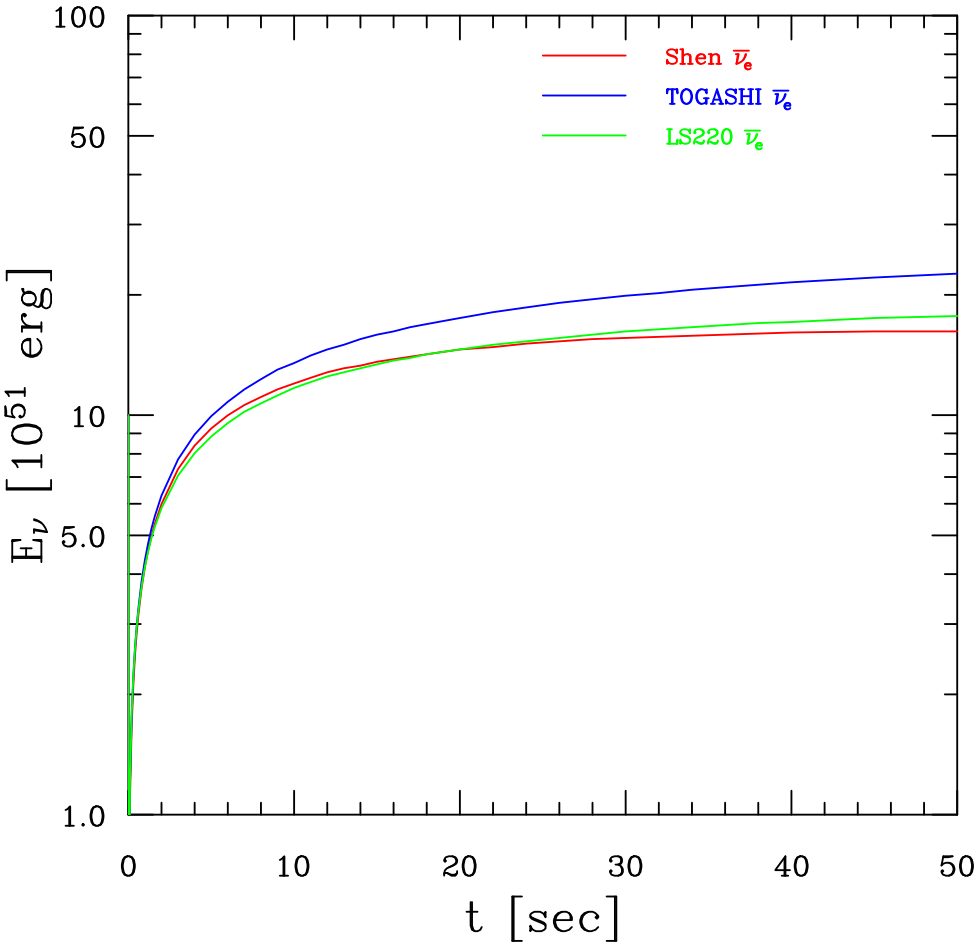

Togashi EOS

原子核実験データから得られた現実的な核力を使った状態方程式

Shen EOS より柔らかく、対称エネルギーも小さい

高温，高密度，高ニュートリノ光度

爆発やニュートリノ観測には好都合